JOURNAL OF DISPERSION SCIENCE AND TECHNOLOGY
Vol. 25, No. 5, pp. 703–712, 2004

# Ocean Disposal of $CO_2$: Conditions for Producing Sinking $CO_2$ Hydrate

**Jorge Gabitto,[1,2] David Riestenberg,[1] Sangyong Lee,[1,#] Liyuan Liang,[1] and Costas Tsouris[1,*]**

[1]Oak Ridge National Laboratory, Environmental Sciences Division, Oak Ridge, Tennessee, USA
[2]Chemical Engineering Department, Prairie View A & M University, Prairie View, Texas, USA

## ABSTRACT

Carbon dioxide sequestration at intermediate ocean depths in the form of a sinking $CO_2$ stream has been shown to be technically feasible. Buoyancy characteristics of $CO_2$ hydrate particles obtained from a coflow reactor operating under conditions that produce negatively buoyant $CO_2$ hydrate composite particles were studied. Using a simplified process model, the limiting ratios of $CO_2$ to water to produce sinking hydrate composite streams were established for pressure and temperature conditions of intermediate ocean depths. A kinetic model involving a mass transfer step and a reaction step was proposed to explain experimental data using a seafloor process simulator. Results suggest that the reactor operates under mass-transfer controlled conditions. Although the density of freshwater is only a few percentage units less than that of seawater, operating conditions derived from freshwater-based studies are significantly different for ambient seawater. Owing to the higher density of seawater, greater conversion of $CO_2$ to hydrate is needed to obtain a sinking $CO_2$ composite stream than at the same depth of freshwater.

*Key Words:* Ocean carbon sequestration; $CO_2$ hydrate; Mass transfer.

## INTRODUCTION

The disposal of anthropogenic greenhouse gases now entering the atmosphere is increasingly becoming a global problem. High atmospheric concentrations of these gases may increase the earth's average temperature and severely modify the world's climate. Carbon dioxide ($CO_2$) is one of the most abundant greenhouse gases. Because of the relatively high solubility of the gas, atmospheric-ocean exchange over the large ocean surface could regulate the atmospheric concentration.[1] Additionally, the large storage capacity of the ocean holds an assurance for an active $CO_2$ injection into the deep ocean to solve this problem.[2,3] For the success of such a strategy, the

[#]Current address: Chemical and Natural Gas Engineering, Texas A&M University Kingsville, Kingsville, TX 78363, USA.
*Correspondence: Costas Tsouris, Oak Ridge National Laboratory, Environmental Sciences Division, Oak Ridge, TN 37831-6181, USA; Fax: (865) 241-4829; E-mail: tsourisc@ornl.gov.



DOI: 10.1081/DIS-200027332
0193-2691 (Print); 1532-2351 (Online)
Copyright © 2004 by Marcel Dekker, Inc.
www.dekker.com

Request Permissions / Order Reprints
powered by RIGHTSLINK

behavior and stability of liquid $CO_2$ after it has been delivered into the ocean are very important.

At pressures above 4.45 MPa and temperatures below 283.4 K, $CO_2$ forms a solid compound with water, known as clathrate or, more commonly, $CO_2$ hydrate.[4] The stability of this solid compound is a function of the temperature and pressure at the disposal depth, where the hydraulic pressure affects the ambient operating pressure, as well as other factors such as constituents in the water reflected in its salinity.[5] The dissolution characteristics of the injected $CO_2$ stream will determine the residence time of the $CO_2$ injected into the sea. Slow dissolution will result in a larger, more dilute $CO_2$ plume, whereas very high dissolution rates of the solid hydrates into seawater will threaten the marine environment by causing an unacceptable decrease in the ocean's pH.[6] Careful design of disposal techniques is required to avoid these problems. The disposal techniques should also be economically feasible; otherwise, they will not be applied in large-scale projects.

Recently, West et al.[7] proposed a technique for direct ocean $CO_2$ injection in which $CO_2$ is disposed of at depths of 1000–1500 m in the form of a negatively buoyant water/liquid $CO_2$/$CO_2$-hydrate composite stream. The sinking characteristics of the composite stream may prolong the $CO_2$ residence time in the ocean during seawater entrainment, mixing, and dispersion by delivering it to greater depths and thus increase the potential for long-term sequestration of $CO_2$ in the ocean.[8]

Based on earlier experimental investigation using both salt water and freshwater, this project determines optimal operating conditions for the process.[7] Simple operating models are proposed to understand the formation process of the composite.

## PREVIOUS EXPERIMENTAL INVESTIGATION

Semisolid $CO_2$ hydrate composites were produced via mixing of liquid $CO_2$ and water in a coaxial cylindrical reactor that was placed in a 72.2-L, temperature-controlled, high-pressure vessel (Fig. 1).[7–9] The coaxial cylindrical reactor (Fig. 2) consists of a capillary tube located at the center of an outer tube. The inner diameter (ID) of this outer tube is 6.3 mm, the ID of the capillary varies between 125 and 250 μm, and the outside diameter of the capillary is 1.6 mm. In the reactor, water is injected at high velocity ($Re = 2100–2900$) through the capillary into a slow-moving stream of liquid $CO_2$ ($Re = 2.2–3.2$).[8] The reactor-mixing zone extends from the outlet of the capillary to the end of the outer tube (~0.14 m).

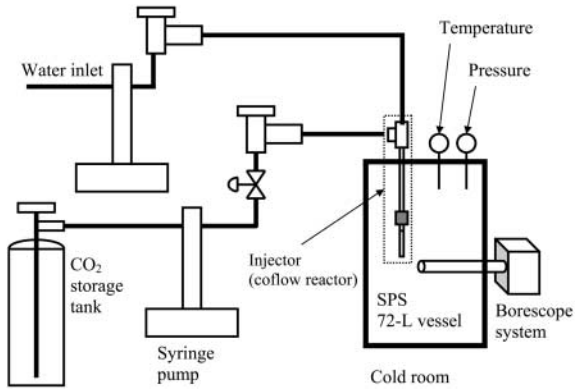


***Figure 1.*** Vessel configuration and experimental arrangement.

Typical experiments involved filling the pressure vessel with fresh water or salt water (3.5% NaCl by weight). The vessel was then pressurized to a predetermined level (10–13 MPa) with nitrogen gas and then cooled to the desired temperature (2–5°C) in a cold room. Liquid $CO_2$ and water were injected using syringe pumps (ISCO, model 100 DM) at predetermined flow rates of 4–20 and 15–25 mL min$^{-1}$, respectively. The composite stream leaving the injector was then observed through a video camera placed against one of the 5-cm sapphire windows of the vessel.[8] The buoyancy of the composite in the surrounding vessel water was observed at various flow rates.

In the injection experiments, water and liquid $CO_2$ were injected into the concentric reactor, where $CO_2$ flowed through the outside annulus, and water was delivered through a central capillary tube (Fig. 1). Water and liquid $CO_2$ were then contacted inside the reactor tube where hydrate formation occurred. Because of hydrodynamic instability of water in liquid $CO_2$, the water phase will break into droplets.[8] Hydrate films form on the water–$CO_2$ interface (Fig. 3) preventing the droplets from coalescing and causing them to cluster together in a "grapelike" configuration (Fig. 2). A large number of droplets appeared to form the solid composite made of hydrate-covered water, unreacted water, and liquid $CO_2$.[8] Both freshwater and saltwater experiments show that at a given vessel pressure and temperature, if the $CO_2$ flow rate is held constant, the buoyancy of the hydrate composite leaving the injector changes from positive to negative with increasing water flow rates (Fig. 4). We also observed that for a given $CO_2$ flow rate, the minimum water flow rate needed to make a sinking composite increased with decreasing pressure.[7,8] However, in saltwater, the minimum water flow rate for making sinking composite hydrate is higher than in freshwater.

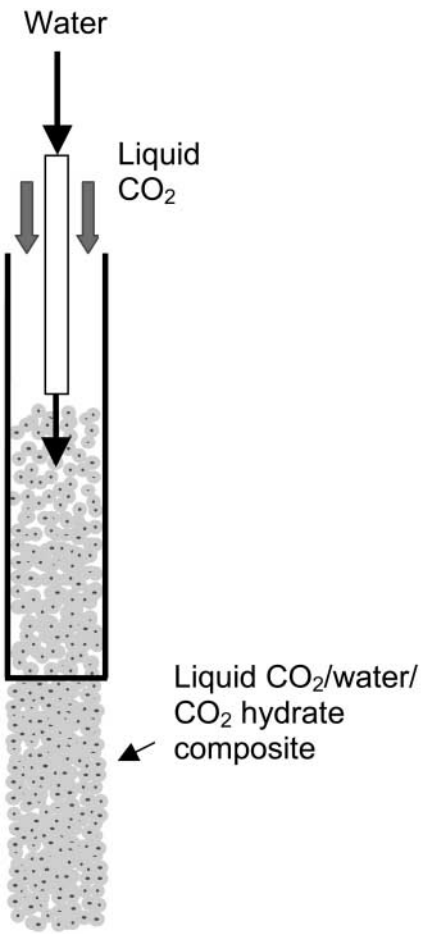


*Figure 2.* Coflow injector.

The presence of water and liquid $CO_2$ will allow further hydrate formation to occur. Because of the non-equilibrium condition of the ambient water, at some point after injection into the surrounding seawater, hydrate dissolution will also become an important process.[10] Since the composite residence time in the reactor is 8–14 sec,[8] this process is assumed not to occur inside the reactor.

## MODEL DEVELOPMENT

Based on the experimental system and observation, a simple model is proposed to study the process with the following assumptions:

1. The limiting reactant is $CO_2$. This assumption is justified based on two facts: (i) $CO_2$ hydrate forms at the water-side of the interface, which means that $CO_2$ has to transfer through hydrate pores and (ii) the flow-rate ratio of $CO_2$ to water in the coflow injections is less than the ratio needed for complete hydrate conversion.
2. Water droplets have sufficient time to fully develop, but they are covered by hydrate shells before there is an opportunity for them to coalesce.[11]
3. All the injected water and liquid $CO_2$ are consumed in forming the hydrate composite, which means no losses of injected liquid phases to the surrounding water.
4. Droplet size can be predicted using liquid–liquid jet hydrodynamic model, as proposed by Teng et al.[11]
5. The hydrate forms on the water-side of the $CO_2$–water interface.[12]

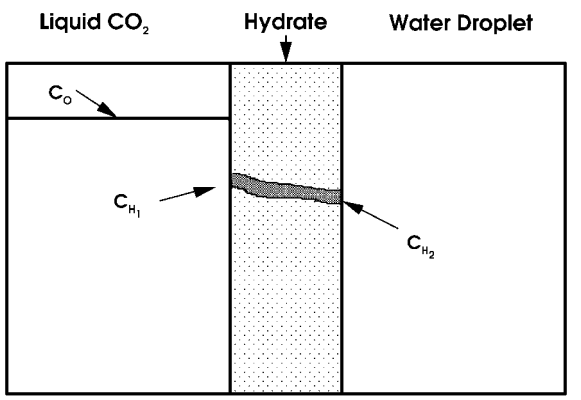


*Figure 3.* Schematic of the kinetic model.

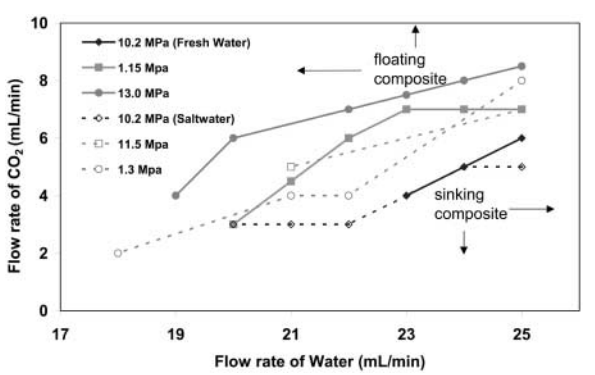


*Figure 4.* Density boundaries for producing negatively buoyant $CO_2$-hydrate composite in freshwater and saltwater. Decreasing the $CO_2$ flow rate or increasing the water flow rate produces a sinking composite. Higher water flow rates are necessary for producing sinking composite in saltwater.

6. The hydrate film slows down mass transfer of $CO_2$ towards the water phase, but does not stop it.[13]
7. The hydrate layer can be considered as a porous solid with the pores filled with water.[14]
8. The entire system works as a chemical reactor with an average conversion, $X$, for the limiting reactant given by

$$X = \frac{F^0_{CO_2} - F_{CO_2}}{F^0_{CO_2}} \tag{1}$$

where $F^0_{CO_2}$ is the initial molar flow of the limiting reactant ($CO_2$) and $F_{CO_2}$ is the exiting molar flow of the limiting reactant.

A mass balance applied to the hydrate composite allows us to derive a relationship between the conversion ($X$) and the hydrate composite density:

$$\rho_{com} = \frac{M_c + M_w \theta^0_w}{\begin{array}{l} M_c/\rho_c(P,T) + M_w \theta^0_w/\rho_w(P,T) \\ \quad + X(M_h/\rho_h(P,T) - M_c/\rho_c(P,T) \\ \quad - n_h M_w/\rho_w(P,T)) \end{array}} \tag{2}$$

Here $\rho_c(P, T)$, $\rho_w(P, T)$, $\rho_h(P, T)$, and $\rho_{com}(P, T)$ are the $CO_2$, water, hydrate, and composite densities, respectively; $M_c$, $M_w$, and $M_h$ are the $CO_2$, water, and hydrate molecular weights, respectively; $n_h$ is the hydrate number (the ratio of water to $CO_2$ molecules in the hydrate); and $\theta^0_w$ is the molar ratio of the input water to input $CO_2$, which is related to $Q_w/Q_{CO_2}$. $Q_w$ and $Q_{CO_2}$ are the operational volumetric flow rates from water and $CO_2$, respectively.

Equation (2) can be used to calculate composite density as a function of limiting reactant conversion and input molar flows at a given ambient temperature and pressure. Equation (2) can be rearranged to obtain the minimum required conversion to produce a composite that is neutrally buoyant ($\rho_{com} = \rho_w$):

$$X_{min} = \frac{(\rho_w(P,T)/\rho_c(P,T) - 1)}{\begin{array}{l} M_h/M_c(\rho_w(P,T)/\rho_h(P,T) - 1) \\ \quad -(\rho_w(P,T)/\rho_c(P,T) - 1) \end{array}} \tag{3}$$

where $X_{min}$ is the conversion value at the neutrally buoyant point (conversion critical point). Although $X_{min}$ is a function of temperature and pressure, it is not a function of the input molar flow ratio, $\theta^0_w$. However, the actual hydrate conversion, $X$, is likely dependant on $\theta^0_w$ because it is expected to influence the mixing of $CO_2$ and water in the reactor and subsequent conversion of $CO_2$ to $CO_2$ hydrate. Other than the minimum conversion, the value of $X$ generally depends on input molar flow ratio.

In order to explore the mechanisms controlling the rate of hydrate formation, we propose a highly simplified kinetic model of this complex process. Although this model may have a limited theoretical foundation, the only purpose of its application is to study qualitatively the kinetics of hydrate formation related to our reactor, and not to propose it for other systems. The kinetic model is based on the assumptions 2, 5, 6, and 7 listed earlier.

The proposed kinetic model is depicted conceptually in Fig. 3. The figure depicts hydrate formation in a single water droplet. The hydrate formation process consists of three steps:

1. $CO_2$ dissolution into pore water at the $CO_2$–hydrate interface.
2. $CO_2$ mass transport through the hydrate porous layer.
3. Reaction at the hydrate–water interface.

The first step involves dissolving $CO_2$ into pore water on the liquid $CO_2$–hydrate interface. The assumption of no mass transfer resistance at this stage of the derivation results in the concentration of pore water $CO_2$ in the hydrate ($C_{H_1}$) at equilibrium with pure liquid $CO_2$ ($C_O$).

$$K_{eq} = \frac{C_O}{C_{H_1}} \tag{4}$$

Here, $K_{eq}$ is the distribution equilibrium constant between the carbon dioxide liquid phase and the liquid water filling the pores of the hydrate layer.

The second step involves mass transfer through the hydrate layer, a process that involves $CO_2$ mass transfer through the water filled pores. This is based on a model presented by Mori and Mochizuki[14] in which the hydrate layer is porous, with water filling the pores and mass transport occurring inside these pores (i.e., liquid diffusion), and not through the solid hydrate (i.e., solid diffusion). The third step represents reaction on the water-side of the hydrate–water interface.

Under steady-state conditions, the rate of every individual step is the same, i.e., the molar flow ($J_c$) of $CO_2$ in all the steps should be the same. A global mass balance on all the particles located inside the reactor yields

$$J_c = K_g C_O V_r = k_{MT} A (C_{H_1} - C_{H_2}) = k_r A C_{H_2} \tag{5}$$

Here, $K_g$ is the overall (global) reaction coefficient, $V_r$ is the reactor volume, $k_{MT}$ is the mass transport coefficient through the hydrate layer, $k_r$ is the reaction rate coefficient at the hydrate–water interface, $A$ is the total reaction area; and all the $C_j$ values are $CO_2$

concentrations at the points shown in Fig. 3, $C_O$ is the concentration of pure $CO_2$ in the liquid phase, $C_{H_1}$ is the aqueous concentration of $CO_2$ in the hydrate pore at equilibrium with liquid $CO_2$, and $C_{H_2}$ is the aqueous concentration of $CO_2$ in the hydrate pore at the hydrate–water interface. The concentration diagram presented in Fig. 3 agrees with those proposed by Ogasawara et al.[15] for $CO_2$ droplet dissolution and by Uchida et al.[16] for hydrate formation in water droplets immersed in liquid $CO_2$.

The linear sequential three-step process described by Eq. (5) allows us to relate the global reaction coefficient ($K_g$) to the mass transfer coefficient through the hydrate layer and to the reaction rate coefficient by the following equation:[17]

$$\frac{K_{eq}}{K_g} = \frac{1}{k_{MT}} + \frac{1}{k_r} \tag{6}$$

The value of $K_g$ can be calculated at the conversion critical points by using our experimental data.[8] The critical conversion values, $X_{min}$, are calculated from Eq. (3), but the critical conversion values can also be calculated using

$$X_{min} = \frac{\text{Reaction rate at critical conversion}}{F^0_{CO}} \tag{7}$$

Introducing Eq. (5) into Eq. (6) yields

$$X_{min} = \frac{K_g A C_O V_r}{F^0_{CO}} \tag{8}$$

Equation (8) allows us to calculate the value of the global reaction rate coefficient, $K_g$, from the experimental data.

## RESULTS AND DISCUSSION

Fluid density generally increases with ambient pressure, depending on the compressibility of the fluid. Because liquid $CO_2$ is more compressible than that of water, its density increases more significantly than water under the same ambient hydraulic pressure at a given ocean depth of water.[8] Figure 5 depicts the density variation for distilled water, saltwater,[18] and $CO_2$[19] with ocean depth. All densities increase as the depth increases.

The critical conversion, $X_{min}$, is defined as the limiting reactant ($CO_2$) conversion that produces neutral buoyancy of the hydrate composite at a given temperature and pressure (or depth) for a given ambient medium. When neutrally buoyant, the density of the hydrate composite is equal to that of surrounding water at that depth. Critical conversion is a function only of

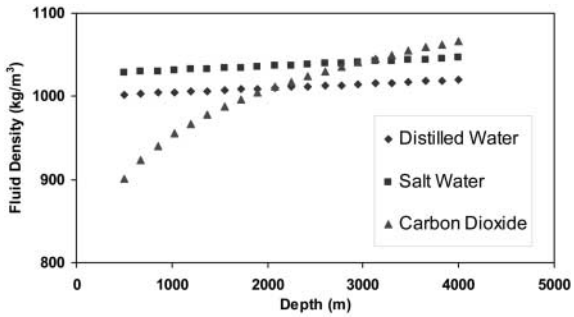


***Figure 5.*** Density variation with depth. Seawater density was provided in Ref. [18] and $CO_2$ density was provided by Teng.[12]

the densities of ambient water, $CO_2$, and solid hydrate, which are functions of temperature and depth. Equation (2) shows that $X_{min}$ values are controlled by the density ratios $\rho_w(P, T)/\rho_c(P, T)$ (for ambient water to liquid $CO_2$) and $\rho_w(P, T)/\rho_h(P, T)$ (for ambient water to hydrate). Figure 6 depicts the variation of the critical conversion with depth for ambient freshwater and saltwater. The critical conversion decreases as depth increases, implying that less $CO_2$ conversion is needed to achieve neutral buoyancy as depth increases. A critical depth is reached when the critical conversion becomes 0. For greater depths, critical conversion values would become negative, which means that neutral buoyancy cannot be achieved at those depths. The reason for this is that the injected fluids are too heavy to maintain neutral buoyancy at depths greater than the critical depth. Although the density difference between freshwater and seawater is small (2–3%), the critical depth is much greater for saltwater (~3000 m) than for freshwater (~2000 m) when used as ambient medium (Fig. 5).

Figure 7 shows that at pressures corresponding to depth values smaller than the critical depth (positive $X_{min}$), the ambient water density is higher than the $CO_2$ density. At the critical depth, $X_{min}$ is equal to 0; therefore,

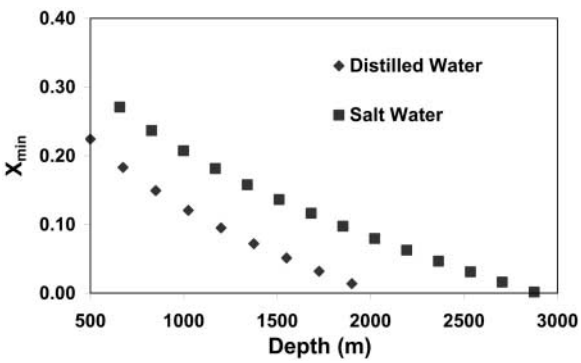


***Figure 6.*** Minimum conversion as a function of depth.

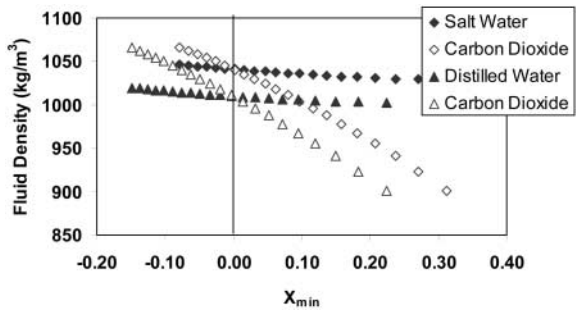


*Figure 7.* Density variation vs. minimum conversion for distilled water and salt water.

the composite consists of water and $CO_2$ only, and the density of the ambient water equals that of $CO_2$, whereas at higher depths the $CO_2$ density becomes higher than the water density. The same behavior was observed using saltwater.

Equation (2) can be used to calculate the density of the produced composite ($\rho_{com}$) at ambient water depth as a function of $CO_2$ conversion. In Fig. 8, which depicts $\rho_{com}/\rho_w$ curves corresponding to different constant conversions, it is apparent that higher conversions associate with higher composite densities. This plot can be used to determine critical conversions for $CO_2$ to produce sinking composite at various water depths. These critical conversion points are determined by the intersections of the conversion curves with the horizontal line $\rho_{com}/\rho_w = 1$. For this calculation, saltwater is used for $\rho_w$.

The influence of the input molar flow of the limiting reactant ($CO_2$) is shown in Fig. 9. The influence of different volumetric flow rate ratios ($Q_w/Q_{CO}$) for $X = 0.1$ is shown. All the curves intersect at one point, independent of the volumetric flow rate ratio of water to $CO_2$. This is the critical conversion point, where $\rho_{com}/\rho_w = 1$, and the corresponding depth depends upon the specific conversion. This behavior was predicted by Eq. (3), in which

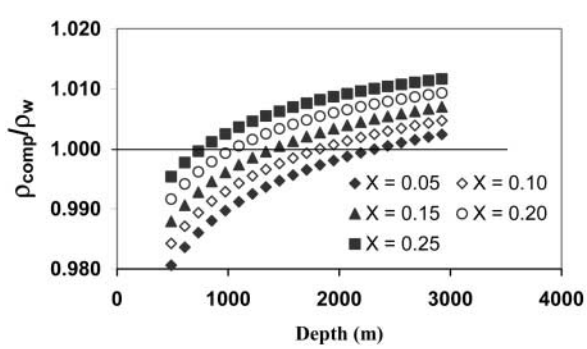


*Figure 8.* Density ratio for constant conversion curves at different depths.

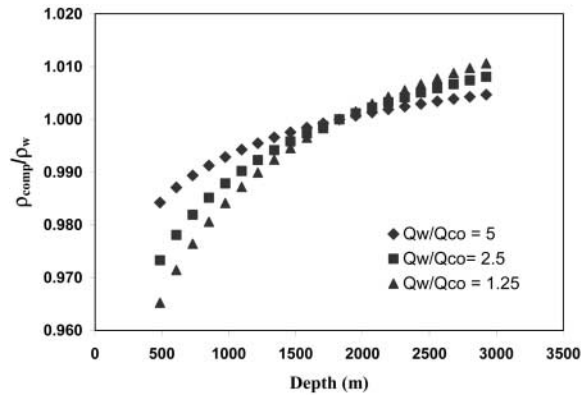


*Figure 9.* Influence of volumetric flow rate ratios ($Q_w/Q_{CO}$) on density ratios for a fixed conversion ($X = 0.1$).

the critical conversion depends only on the phase densities, but not on the feed ratios of the two reactants. This behavior is not observed for other depth values, as shown in Fig. 9. At less than the critical conversion depths, the density ratios are higher for higher water to $CO_2$ volumetric flow rate ratios. However, this trend is reversed for depths values higher than the one corresponding to the critical conversion point. This finding can be explained by considering that at lower depths than the one corresponding to the critical conversion point, the density of water is higher than that of $CO_2$, but the reverse is true at greater depth values.

Figure 10 shows that higher conversions ensure higher densities operating under constant volumetric flow rate ratios. The density of the critical conversion point has been determined experimentally by recording the water density at the corresponding pressure and temperature.[8] The volumetric flow rate ratios corresponding to the different critical conversion points were also determined experimentally. After the determination

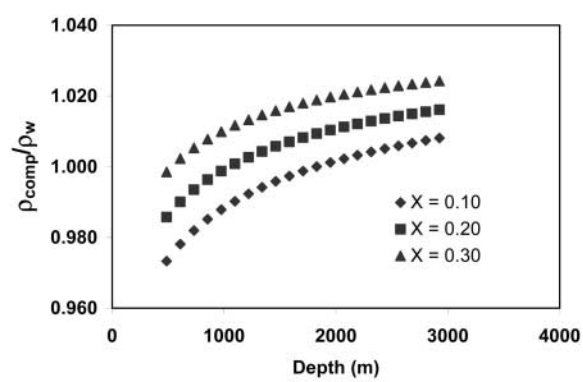


*Figure 10.* Density ratio variation with depth at different conversions using a constant volumetric feed ratio $\theta_w^0 = 2.5$.

of the volumetric flow rate ratio corresponding to the critical conversion point, further increases in the $CO_2$ flow rate produced a positively buoyant composite, whereas decreases in the volumetric flow of $CO_2$ produced negatively buoyant (sinking) hydrate composite. Of course, the density of the positively buoyant composite is lower than the ambient water density, whereas the density of the sinking hydrate is higher than that of the surrounding seawater. It is reasonable to assume that negatively buoyant hydrate composite will have conversion values above the critical value, whereas positively buoyant hydrate will have conversion values below the critical value. This conclusion is supported by Fig. 10, which shows that for the same depth, higher density values are associated with higher conversion values. A clear example is a depth of 1000 m, where the critical conversion is approximately 0.2 ($\rho_{com}/\rho_w = 1$). A conversion of 0.3 predicts a density ratio greater than 1, whereas a conversion of 0.1 predicts a density ratio below 1.

A method for experimental determination of the density values for composites produced in coflow injections showing buoyancy behavior other than the neutral buoyancy at critical conversion has not yet been developed; therefore, qualitative calculations were performed using Eqs. (2) and (3). We started with the experimentally determined composite density obtained at the critical conversion point [Eq. (3)], and then set several values of density and volumetric ratio above and below the critical ones. The main idea was to test the sensitivity of Eqs. (2) and (3) to volumetric flow ratio ($\theta_w^0$) and density values. Values of volumetric flow ratio ($\theta_w^0$) and density values were proposed and the corresponding conversions were calculated using Eq. (2). Typically, four values of volumetric ratios ($\theta_w^0$) were calculated, 5% and 10% higher and 5% and 10% lower than critical. Corresponding density values, 0.3% and 0.5% higher and 0.3% and 0.5% lower than the critical density, were proposed and also used. It should be noted that due to the sensitivity of Eqs. (2) and (3), small density changes produce large changes in the values of the conversion.

Examples for three different points are shown in Table 1. The positively buoyant values are indeed associated with conversions below the critical ones, whereas the negatively buoyant values are associated with conversions above the critical conversion point. Large changes in conversion produce small changes in density, and the sensitivity of the equation suggests the need for very careful design of these reactors. Small local density changes could require operating conversions very different from the predicted ones.

The product of minimum conversion ($X_{min}$) and $CO_2$ input molar flow ($F_{CO_2}^0$) represents the amount of $CO_2$ converted in the reactor for neutrally buoyant particles. Figure 11 shows the increase of the global reaction rate coefficient ($K_g$) as the amount of converted $CO_2$ is increased. The plot is a graphical representation of Eq. (8). Small discrepancies between the experimentally derived (discrete points) and calculated (straight line) with Eq. (8) are due to inaccuracies in determining the total surface area ($A$) of the particles (8) and the $CO_2$ concentration ($C_O$).

The relationship between the value of the global reaction rate coefficient and the water-phase Reynolds

***Table 1.*** Density differences for conversion changes.

| $P$ (MPa) | $T$ (°C) | $Q_w/Q_{CO_2}$ | $X$ | Density (kg m$^{-3}$) | Buoyancy behavior |
|---|---|---|---|---|---|
| 10.5 | 277.5 | 5.45 | 0.038 | 1000.1 | Positively buoyant |
| 10.5 | 277.5 | 5.71 | 0.067 | 1002.2 | Positively buoyant |
| 10.5 | 277.5 | 6.00 | 0.116 | 1005.2 | Neutral |
| 10.5 | 277.5 | 6.30 | 0.169 | 1008.2 | Negatively buoyant |
| 10.5 | 277.5 | 6.60 | 0.208 | 1010.2 | Negatively buoyant |
| 11.8 | 277.85 | 2.99 | 0.049 | 1000.8 | Positively buoyant |
| 11.8 | 277.85 | 3.13 | 0.067 | 1002.8 | Positively buoyant |
| 11.8 | 277.85 | 3.29 | 0.098 | 1005.8 | Critical |
| 11.8 | 277.85 | 3.45 | 0.130 | 1008.8 | Negatively buoyant |
| 11.8 | 277.85 | 3.61 | 0.154 | 1010.9 | Negatively buoyant |
| 13.2 | 278.2 | 4.32 | 0.012 | 1001.5 | Positively buoyant |
| 13.2 | 278.2 | 4.52 | 0.037 | 1003.5 | Positively buoyant |
| 13.2 | 278.2 | 4.75 | 0.079 | 1006.5 | Critical |
| 13.2 | 278.2 | 4.99 | 0.124 | 1009.5 | Negatively buoyant |
| 13.2 | 278.2 | 5.23 | 0.157 | 1011.5 | Negatively buoyant |

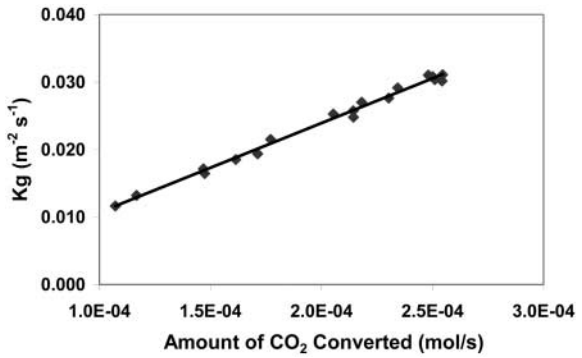


*Figure 11.* Variation of global reaction rate coefficient with amount of $CO_2$ converted for freshwater experiments.

number is depicted in Fig. 12 for both freshwater and saltwater (3.5% NaCl) injections. An increase in Reynolds number produces an increase in the value of the global rate coefficient $K_g$. The global rate coefficient is a function of a mass transfer coefficient ($k_{MT}$) and a reaction rate coefficient ($k_r$), as shown in Eq. (6). As the increasing of the Reynolds number implies greater mixing and mass transfer, results in Fig. 12 suggest that our reactor is operating under mass transport-controlled conditions ($k_r \gg k_{MT}$). Therefore, an increase in the mass transfer rate through the hydrate layer can be expected as the Reynolds number increases.

Mass transfer through the hydrate layer occurs mostly through pores of different sizes (Fig. 3). This process is very complex and depends on several non-measurable parameters.[14] A possible explanation is that the assumption of equilibrium conditions at the $CO_2$–hydrate interface is not realistic. In this case, the $CO_2$ concentration at the interface ($C_{H_i}$) will be below the equilibrium value and its real value would be determined by the dynamic conditions inside the reactor.

If we assume that the global reaction rate is controlled by the mass transfer step, we can use Eq. (3) to calculate the mass transfer coefficient ($k_{MT}$). Figure 13 shows that the mass transfer coefficient increases linearly with the Reynolds number within the range studied.

Unfortunately, neither the mass transfer coefficient through the hydrate layer ($k_{MT}$) nor the specific reaction rate coefficient ($k_r$) can be determined independently in a reliable way. Ogasawara et al.[15] reported mass transfer coefficient values with and without hydrate layer for dissolution of individual $CO_2$ drops moving at their terminal velocities. The authors measured mass transfer coefficient values in the presence of a hydrate layer ($k_{MT}$), and found them to vary around $10^{-6}\,\mathrm{m\,sec^{-1}}$. Because of the differences between experiments of Ogasawara et al.[15] and our own investigations, only a limited comparison between Ogasawara's results and the ones calculated in this work was attempted. The calculated values using Eq. (6) are approximately an order of magnitude smaller than those reported by Ogasawara et al.[15] (Fig. 13). The comparison is not unfavorable, considering the uncertainties in the literature results and the error associated with our experiments. The presence of a "swarm" of drops,[8] instead of a single one, should also contribute to the lower values for mass transfer coefficients calculated in this work.

Caution should be exercised in making assumptions based on the kinetic information reported here. The range of Reynolds numbers studied is too narrow, and the experimental data showed significant spread. However, our results suggest definite trends. Similar trends were observed for experimental data for saltwater (Fig. 12). The density difference between saltwater and freshwater requires higher conversion values to produce negatively buoyant hydrate. The slope of the global reaction coefficient ($K_g$) vs. total Reynolds number appears to be

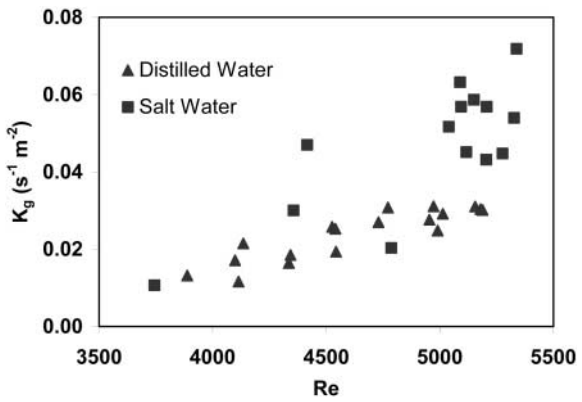


*Figure 12.* Variation of global reaction rate coefficient with Reynolds number for saltwater and freshwater.

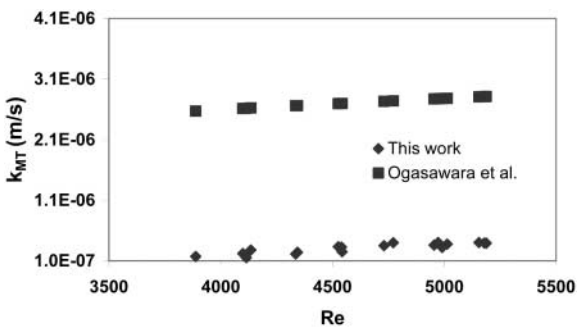


*Figure 13.* Estimated mass transfer coefficient values for freshwater experiments as a function of Reynolds number.

steeper for the experimental saltwater data than that for the fresh water. The differences between the two sets of data are greater at high flows than at low ones. This behavior suggests the presence of an ionic effect on the value of the reaction rate coefficient. However, in our opinion, the lack of true kinetic values precludes a thorough analysis of these experimental results, and the observed trends are presented without any attempt to draw unsupported conclusions.

## CONCLUSIONS

A simple model was developed to predict the minimum $CO_2$ conversion necessary to produce negatively buoyant hydrate (i.e., the critical conversion point) for a given ambient water medium at a given pressure and temperature. The minimum $CO_2$ conversion decreases as the disposal depth increases, and higher $CO_2$ conversion increases the density of the hydrate composite. The values for both minimum conversion and disposal depth are very sensitive to density changes. Laboratory operating conditions determined using freshwater can be very different from the same conditions determined using saltwater. At the critical conversion point, the minimum $CO_2$ conversion does not depend upon feed ratios of water and $CO_2$. However, above and below the critical point, density ratios are strongly dependent upon feed ratios. Multiple feed ratios of $CO_2$ to water produce sinking hydrate for fixed temperature and pressure values. A model including a mass transport step through the hydrate layer and reaction on the waterside of the interface can be used to study the reactor performance. The hydrate layer can be represented as a porous material with the pores filled with water. The experimental data suggest that near critical conversion points, the process is mass transport limited, indicating that better mixing conditions may lead to higher conversion. The difference between the global reaction rate coefficient values ($K_g$) for experiments in freshwater and simulated saltwater suggests an ionic effect on the mass transport rate.

## NOMENCLATURE

| | |
|---|---|
| $A$ | mass transfer area ($m^2$) |
| $C_O$ | pure liquid $CO_2$ concentration ($mol\,L^{-1}$) |
| $C_{H_1}$ | $CO_2$ concentration in hydrate pore ($mol\,L^{-1}$) |
| $C_{H_2}$ | $CO_2$ concentration on the water-side ($mol\,L^{-1}$) |
| $F_i$ | molar flow in/out of the reactor of component $i$ ($mol\,sec^{-1}$) |
| $J_c$ | molar flow ($mol\,sec^{-1}$) |
| $k_{MT}$ | mass transfer coefficient ($m\,sec^{-1}$) |
| $k_r$ | reaction rate coefficient ($m\,sec^{-1}$) |
| $K_{eq}$ | $CO_2$/water equilibrium constant |
| $K_g$ | global reaction rate coefficient ($m^{-2}\,sec^{-1}$) |
| $M_i$ | molecular weight of component $i$ ($g\,mol^{-1}$) |
| $n_h$ | the hydrate number |
| $P$ | pressure ($m^{-1}\,kg\,sec^{-2}$) |
| $Q$ | volume flow rate of component $i$ ($m^3\,sec^{-1}$) |
| $\rho_i$ | density of component $i$ ($kg\,m^{-3}$) |
| $T$ | temperature (K) |
| $\theta_w^0$ | input water/$CO_2$ volume flow ratio ($Q_w/Q_{CO_2}$) |
| $V_r$ | reactor volume ($m^3$) |
| $X$ | conversion |

### Subscripts

| | |
|---|---|
| CO | $CO_2$ |
| com | composite |
| h | hydrate |
| w | water |

## REFERENCES


1. Takahashi, T.; Feely, R.A.; Weiss, R.F.; Wanninkhof, R.H.; Chipman, D.W.; Sutherland, S.C.; Takahashi, T.T. Global air–sea flux of $CO_2$: an estimate based on measurements of sea–air $pCO_2$ difference. Proc. Natl. Acad. Sci. **1997**, *94*, 8292–8299.
2. Reck, R.A.; Hoag, K.J. A comparison of greenhouse gas mitigation options. Energy **1997**, *22*, 115–120.
3. U.S. Department of Energy. *Carbon Sequestration Research and Development*; Office of Science and Office of Fossil Energy: Washington, DC, 1999.
4. Lee, S.-Y.; Holder, G.D. Model for gas hydrate equilibria using a variable reference chemical potential: Part 1. AIChE J. **2002**, *48*, 161–167.
5. Sloan, E.D. *Clathrate Hydrates of Natural Gases*; Marcel Dekker: New York, 1998.
6. Tamburri, M.N.; Peltzer, E.D.; Friederich, G.E.; Aya, I.; Yamane, K.; Brewer, P.G. A field study of the effects of $CO_2$ ocean disposal on mobile deep-sea animals. Mar. Chem. **2000**, *72*, 95–101.
7. West, O.; Tsouris, C.; Liang, L.; Lee, S.Y.; McCallum, S. Negatively buoyant $CO_2$-hydrate composite for ocean carbon sequestration. AIChE J. **2003**, *49*, 283–285.
8. Lee, S.Y.; Liang, L.; Riestenberg, D.E.; West, O.R.; Tsouris, C. $CO_2$-hydrate composite for ocean carbon

sequestration. Environ. Sci. Technol. **2003**, *37*, 3701–3708.
9. Phelps, T.; Peters, D.J.; Marshall, L.S.; West, O.R.; Liang, L.; Blencoe, J.G.; Alexiades, V.; Jacobs, G.K.; Naney, M.T.; Heck, J.L., Jr. A new experimental facility for investigating the formation and properties of gas hydrates under simulated seafloor conditions. Rev. Sci. Instrum. **2001**, *72*, 1514–1521.
10. Teng, H.; Yamasaki, A. Can $CO_2$ hydrate deposited in the ocean always reach the seabed? Energ. Convers. Manage. **1998**, *39*, 1045–1051.
11. Teng, H.; Kinoshita, C.M.; Masutani, S.M. Prediction of droplet size from the breakup of cylindrical liquid jets. Int. J. Multiphas. Flow **1995**, *21*, 129–136.
12. Teng, H. Characteristics of the hydrate layer formed at the liquid $CO_2$–water interface. Int. J. Chem. Kinet. **1996**, *28*, 935–937.
13. Teng, H.; Yamasaki, A. Mass transfer of $CO_2$ through liquid $CO_2$–water interface. Int. J. Heat Mass Tran. **1998**, *41*, 4315–4325.
14. Mori, Y.H.; Mochizuki, T. Mass transport across clathrate hydrate films—a capillary permeation model. Chem. Eng. Sci. **1997**, *52*, 3613–3616.
15. Ogasawara, K.; Yamasaki, A.; Teng, H. Mass transfer from $CO_2$ drops traveling in high-pressure and low-temperature. Water. Energ. Fuel. **2001**, *15*, 147–150.
16. Uchida, T.; Ebinuma, T.; Kawabata, J.; Narita, H.J. Microscopic observations of formation processes of clathrate hydrate films at an interface between water and carbon dioxide. J. Cryst. Growth, **1999**, *204*, 348–356.
17. Welty, J.R.; Wicks, C.E.; Wilson, R.E. *Fundamentals of Momentum, Heat and Mass Transfer*; John Wiley & Sons, Inc.: New York, 1969; Chapter 26, Sec. 2.
18. Teng, H.; Yamasaki, A.; Shindo, Y. The fate of liquid $CO_2$ disposed of in the ocean. Energy **1996**, *21*, 765–774.
19. Reid, R.C.; Prausnitz, J.M.; Poling, B.E. *The Properties of Gases and Liquids*; McGraw-Hill: New York, 1987.

Received December 4, 2003
Accepted February 18, 2004